Journal of Applied Polymer Science

Synthesis of Fe_3O_4@SiO_2@MPS@P4VP nanoparticles for nitrate removal from aqueous solutions

Farzad Javaheri, Shadi Hassanajili
Department of Chemical Engineering School of Chemical and Petroleum Engineering, Shiraz University, Shiraz 71348-51154, Iran
Correspondence to: S. Hassanajili (E-mail: ajili@shirazu.ac.ir)

ABSTRACT: In this study, synthesis of Fe_3O_4@SiO_2@MPS@poly(4-vinylpyridine) core-shell-shell structure was investigated as an efficient adsorbent for removal of nitrate ions from aqueous solutions. Fe_3O_4 nanoparticles were initially prepared by co-precipitation method, then the surface of Fe_3O_4 was coated with SiO_2 through a modified St öber method. Finally, the Fe_3O_4@SiO_2 nanoparticles were modified by 3-(trimethoxysilyl) propyl methacrylate followed by emulsion polymerization of 4-vinylpyridine. The resultant material was acidified in HCl solution to be effective for nitrate removal. The synthesized sample was characterized by X-ray diffraction, transmission electron microscopy, field-emission scanning electron microscopy, Fourier-transform infrared spectra, thermogravimetric analysis (TGA), and vibrating sample magnetometer. The removal efficiency was optimized for some experimental parameters such as pH, contact time, and amount of sorbent loading. The maximum predictable adsorption capacity was 80.6 (mg nitrate/g sorbent) at optimum conditions. Also, regeneration of the nitrate adsorbed particles was possible with NaOH solution. © 2016 Wiley Periodicals, Inc. J. Appl. Polym. Sci. **2016**, *133*, 44330.

KEYWORDS: composites; grafting; nanoparticles; nanostructured polymers; nanowires and nanocrystals

Received 8 January 2016; accepted 2 August 2016
DOI: 10.1002/app.44330

INTRODUCTION

Nitrate is commonly one of the important source of ground and surface waters pollutant. Nitrate in drinking water is often due to human activities such as excessive use of chemical fertilizers and inappropriate disposal of industrial wastes.[1] High concentrations of nitrate in groundwater can lead to eutrophication of water supplies.[2] Furthermore, exposure to high levels of nitrates causes methemoglobinaemia ("blue baby" syndrome) in infants and health problems such as formation of carcinogenic nitrosamines in adults.[3] Because of the harmful risks related to nitrate, World Health Organization has adopted an allowable level of nitrate concentration of 50 mg NO_3^-/L.[4] Many treatment techniques such as adsorption,[5] reverse osmosis,[6] ion exchange,[7] nanofiltration,[8] electrodialysis,[9] chemical and biological denitrification[10,11] have been applied for the removal of nitrate from water. The conventional techniques are relatively expensive and produce large amount of sludge. Therefore, adsorption has been frequently studied due to its simplicity, cost effectiveness, variety of adsorbents, and low sludge production.[12] Due to unique properties of magnetic nanoparticles including high surface area, ease of separation using external magnetic field and ability of surface modification; magnetic nanoparticles could be considered as effective adsorbents. Poursaberi *et al.*[13] used magnetic nanoparticles modified with 3-aminopropyl-triethoxysilane followed by oxovanadium(IV) porphyrin to remove nitrate ions from aqueous solutions. The adsorbent showed a good efficiency in nitrate extraction and regeneration of nitrate adsorbed material was possible with NaOH solution. Ghasemi *et al.*[14] removed nitrate and nitrite ions from environmental samples using hydroxyapatite-coated γFe_2O_3 nanoparticles. Under the optimum conditions, the adsorption efficiencies of magnetic hydroxyapatite nanoparticles toward nitrate and nitrite ions were about 93%. Nabid *et al.*[15] synthesized nanocomposites of multi-walled carbon nanotubes with conducting polymers such as polyaniline, polypyrrole, poly (1,8-diaminonaphthalene) and poly(2-vinylpyridine) for removing nitrate from drinking water using ion exchange mechanism. Due to negative charge of nitrate ions, a cationic adsorbent can easily adsorb nitrate ions. Poly(4-vinylpyridine) (P4VP) is one of the cationic polymers that widely used as adsorbent,[16] catalyst,[17,18] resins,[19] membrane,[20] oxidizing and reducing agents.[21,22] According to our literature survey, no effort has been yet conducted to use P4VP/magnetic nanoparticles for nitrate removal from aqueous solutions. In this study, poly(4-vinylpyridine) was grafted to the surface of modified magnetic nanoparticles for adsorption of nitrate ions through ion-exchange mechanism. Grafting-from polymerization technique was used for *in situ*

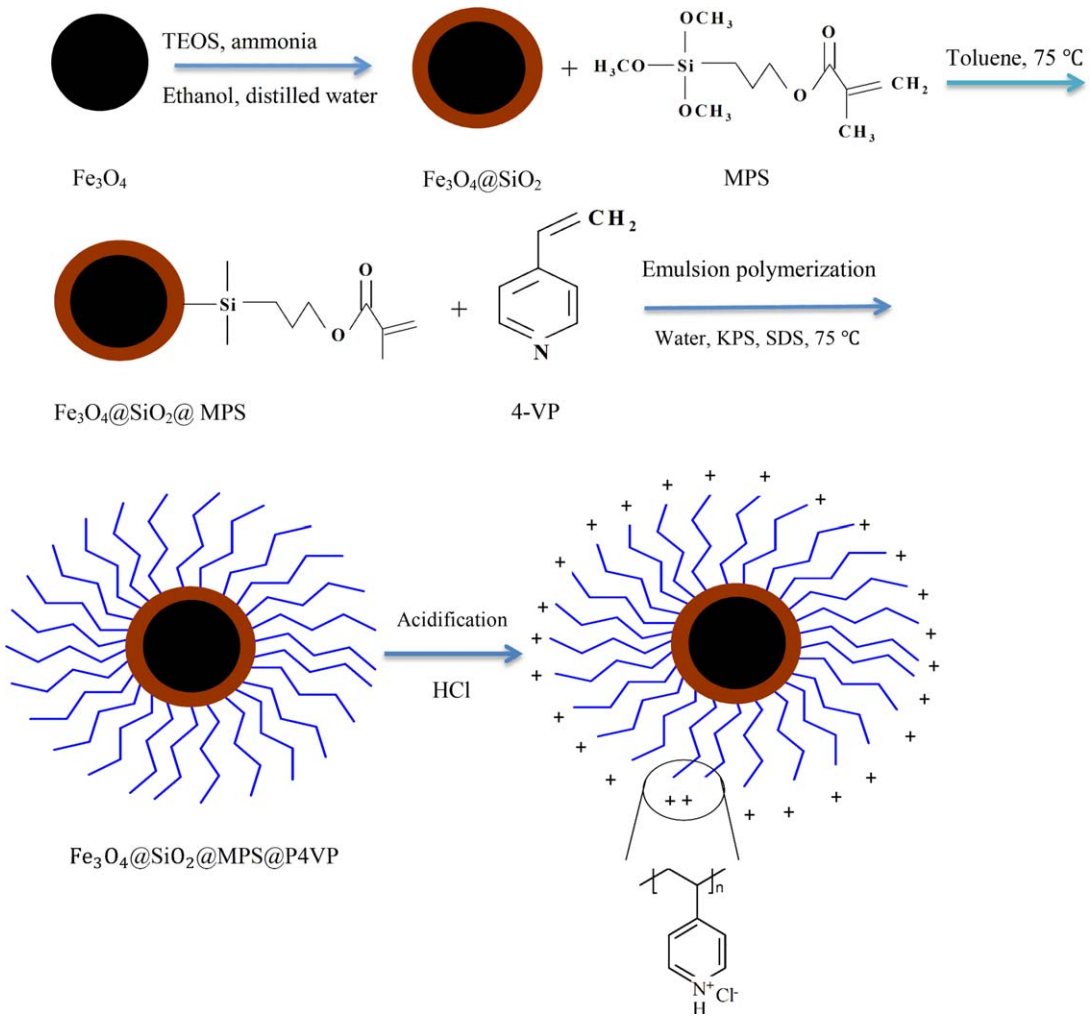

Figure 1. Schematic of Fe_3O_4@SiO_2@MPS@P4VP nanospheres synthesis. [Color figure can be viewed at wileyonlinelibrary.com.]

generation and covalent attachment of P4VP onto the magnetic substrate. First, the magnetic nanoparticles were prepared by co-precipitation method. Then, Fe_3O_4 nanoparticles were coated with a thin layer of SiO_2 through a modified Stöber method. Finally, the Fe_3O_4@SiO_2 nanoparticles were immobilized by 3-(trimethoxysilyl) propyl methacrylate (MPS) as an initiator controller agent followed by *in situ* free radical polymerization of 4-vinylpyridine in water. The resultant material was subjected to the acidification procedure, before its use as an adsorbent for the effective removal of nitrate ions. Ease of separating adsorbent from solution due to magnetic property of cores, using cationic polymer with large amount of active sites and higher value of adsorption capacity compared to other studies are main advantages and novelty of this work.

EXPERIMENTAL

Materials

Ferric chloride hexahydrate ($Fe\ Cl_3.6H_2O$), ferrous chloride tetrahydrate ($FeCl_2.4H_2O$), tetraethyl orthosilicate (TEOS), ammonia solution (25 wt %), ethanol (C_2H_5OH), toluene ($C_6H_5CH_3$), potassium persulfate (KPS), and sodium dodecyl sulfate (SDS) were purchased from Merck & Co. MPS (98%) and 4-vinylpyridine monomer (4-vp, 95%) were purchased from Sigma-Aldrich. Distilled water was used in whole experiment.

Preparation of Fe_3O_4@SiO_2 Nanoparticles

Fe_3O_4 nanoparticles were prepared by co-precipitation method.[23] At first, 1g of $FeCl_2$ and 2.7g of $Fe\ Cl_3$ were dissolved in 400 mL of nitrogen degassed distilled water in a three-necked flask. Then, 10 mL of ammonia solution were added dropwise to the solution under vigorous stirring at 65 °C. The obtained Fe_3O_4 particles was separated with a magnet and washed with distilled water and ethanol. Finally, the precipitant was dried at 60 °C for 6 h. Fe_3O_4@SiO_2 nanoparticles with a core-shell structure were prepared by modifying the Stöber method.[24] Briefly, 0.5 g of Fe_3O_4 was homogeneously dispersed in the mixture containing 160 mL of ethanol, 40 mL of distilled water, and 10 mL of ammonia by ultrasonication. Then, 0.8 mL of TEOS was slowly added to this dispersion. The resulting mixture was stirred at 600 rpm for 6 h at ambient temperature. The resultant Fe_3O_4@SiO_2

nanoparticles were separated with a magnet and washed with ethanol, followed by drying at 60 °C for 12 h.

Modification of Fe_3O_4@SiO_2 Nanoparticles by MPS

Fe_3O_4@SiO_2 nanoparticles were homogeneously dispersed in 120 mL of toluene by ultrasonication and added to a three-necked flask under a nitrogen atmosphere. A certain amount of MPS (4 mL) was dissolved in 10 mL of ethanol while stirring, followed by adjusting pH of the solution to 4 with HCl. Then, it was slowly added into the flask. The mixture was refluxed at 75 °C and mechanically stirred for 6 h. The MPS-modified Fe_3O_4@SiO_2 nanoparticles were collected by a magnet and washed with ethanol three times to remove excess MPS and dried at 60 °C for 12 h.

Synthesis of Fe_3O_4@SiO_2@MPS@P4VP Nanospheres

Fe_3O_4@SiO_2@MPS@P4VP nanospheres were prepared by emulsion polymerization. First, 1 g of MPS-modified Fe_3O_4@SiO_2 nanoparticles were homogeneously dispersed in a solution containing 100 mL water and 80 mg of SDS. Then, 0.4 mL of 4-vp monomer (3.7 mmol) was added to certain amount of ethanol and were injected into the solution. The obtained mixture was homogenized by ultrasonication for 20 min and moved to a four-necked flask equipped with condenser and mechanical stirrer under N_2 gas. After 30 min stirring, the temperature was raised to 75 °C, 2 mL of KPS solution (0.02 g/mL) was injected into the solution to initiate the polymerization. After 6 h, the obtained Fe_3O_4@SiO_2@MPS@P4VP nanospheres were cooled to room temperature, then were collected by magnet and washed with ethanol to remove unreacted materials. Finally, the product dried in vacuum oven at 60 °C for 12 h. The grafting yield (G) was determined by the following equation:

$$G(\%) = 100 \times \frac{w_g - w_0}{w_0} \quad (1)$$

where w_g and w_0 are the weights of the grafted and magnetic nanoparticles, respectively. The yield of the polymer grafting was about 20%. Furthermore, elemental analysis performed on Fe_3O_4@SiO_2@MPS@P4VP revealed that nearly 40% of the 4VP monomers initially contacted with the magnetic nanoparticles were effectively grafted on Fe_3O_4@SiO_2@MPS surface. Therefore, the actual amount of grafted 4VP groups was 1.45 mmol/g sorbent material. Finally, the obtained particles was acidified in HCl solution (0.1 M) to be effective for the removal of nitrate ions. Figure 1 illustrates the synthesis procedure of nanospheres.

Fourier-transform infrared spectra (FTIR) spectra were measured in the wavenumber range from 400 to 4000 cm^{-1} using a Shimadzu 8000 FTIR spectrophotometer with resolution 4 cm^{-1} using the KBr pellet technique. The particle size and morphology of the particles were obtained using Hitachi 1460 field-emission scanning electron microscopy (FE-SEM) and Philips CM30 TEM. Particle size distribution of nanoparticles was obtained by a particle size analyzer (PSA) instrument (JAPA Horiba LB 550). The crystalline structure of the nanoparticles was characterized by X-ray diffraction (XRD) using a Bruker D8 advance X-ray diffractometer. The magnetic properties were measured using a. Magnetization measurements were obtained at room temperature using a vibration sample magnetometer (VSM; Kavir Magnet Company, Iran). Thermogravimetric analysis (TGA) thermograms were recorded on an instrument of Mettler Toledo TGA. Nitrate ions were analyzed using a Genesys 10UV spectrophotometer. Zeta potential measurements were performed using a ZetaPals zeta potential analyzer BIC (Brookhaven Inst. Corp.) A diluted aqueous solution (~1.5 mg/mL) of Fe_3O_4@SiO_2@ P4VP was measured before and after the acidification. The water contact angle (WCA) of nanoparticles was determined with a DSA100 CA analyzer (Krüss, Germany) to characterize the surface property of Fe_3O_4@SiO_2@P4VP nanoparticles before and after the acidification. Before measurements, the nanoparticles were placed on a slide and pressed into a flat film.

Adsorption Experiments

The adsorption ability of synthesized nanosorbent for nitrate ions was investigated using aqueous solutions of KNO_3. Removal of nitrate by nanosorbent has been studied in batch experiments. A known amount of nanosorbent was mixed with specific nitrate solutions, after adequate time nanosorbent was magnetically removed by a magnet and final nitrate concentration was determined by a UV spectrophotometer.

The percentage removal (Re) of nitrate was calculated according to eq. (2):

$$Re\,(\%) = \frac{C_i - C_e}{C_i} \times 100 \quad (2)$$

where C_i and C_e are the initial and equilibrium concentration of nitrate ions before and after sorption. Effect of such parameters on nitrate removal was investigated under the following conditions: pH: 2–10, contact time: 10–180 min, and sorbent dosage: 10–80 mg. The initial concentration of samples was 100 ppm and whole experiment were taken in a 10 mL beaker. Equilibrium adsorption of nanosorbent (in unit of mg nitrate per g of sorbent) was calculated using:

$$q_e = (C_i - C_e) \times \frac{V}{m} \quad (3)$$

where q_e (mg/g) is the adsorption capacity, C_i and C_e (mg/L) are the initial and equilibrium concentration of nitrate ions, V (L) is the volume of nitrate solution, and m (mg) is the mass of the sorbent added.

Several isotherm models have been proposed to evaluate the equilibrium adsorption, among them Langmuir and Freundlich models are the most common. These models describe the equilibrium between adsorbent and adsorbate at constant temperature. The Langmuir model assumes that only monolayer adsorption occurs on the surface, adsorbent surface has certain number of active sites and each site can attract only one species. This model describe as:

$$q_e = \frac{K_L C_e}{1 + a_L C_e} \quad (4)$$

where K_L and a_L are the Langmuir constants. The linearized form of this model is:

$$\frac{C_e}{q_e} = \frac{1}{q_m a_L} + \frac{C_e}{q_m},\ q_m = \frac{K_L}{a_L}. \quad (5)$$

where q_m (mg/g) is maximum adsorption capacity. Freundlich isotherm is another form of Langmuir model that express heterogeneous levels. Freundlich isotherm describe as:

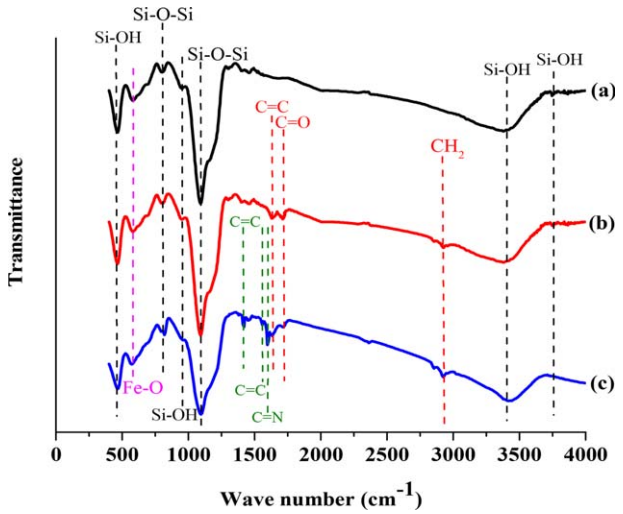

Figure 2. FTIR spectra of (a) Fe_3O_4@SiO_2, (b) Fe_3O_4@SiO_2@MPS, and (c) Fe_3O_4@SiO_2@MPS@P4VP. [Color figure can be viewed at wileyonlinelibrary.com.]

$$q_e = KF\, C_e^{1/n} \tag{6}$$

where K_F and n are the Freundlich constants. The linearized form of Freundlich isotherm is:

$$\ln q_e = \ln KF + \frac{1}{n} \ln C_e \tag{7}$$

RESULTS AND DISCUSSION

Characterization of Synthesized Nanoparticles

The FTIR spectra of (a) Fe_3O_4@SiO_2, (b) Fe_3O_4@SiO_2@MPS, and (c) Fe_3O_4@SiO_2@MPS@P4VP are shown in Figure 2. From Figure 2, Fe–O vibration band at 594 cm^{-1} can be found obviously. In Figure 2(a), the characteristic bands at 1080 and 794 cm^{-1} are associated with the amorphous silica Si—O—Si vibration, and the band at 960 cm^{-1} is attributed to the Si—OH vibration.[25,26] The presence of these peaks confirms that Fe_3O_4 nanoparticles were coated with SiO_2. Furthermore, the very wide absorption band observed at 3431 cm^{-1} is due to hydrogen-bonded Si—OH in the presence of physically adsorbed water while the weak absorption band at 3740 cm^{-1} is attributed to free Si—OH groups.[27]

In Figure 2(b), new bands appear at 2890, 1712, and 1635 cm^{-1} are associated to stretching vibration of CH_2, C=O and C=C groups of MPS, respectively.[28] In Figure 2(c), the absorption peak at 1596 cm^{-1} is related to stretching vibration of C—N bond of the pyridine ring and two peaks at 1420 and 1550 cm^{-1} are assigned to C=C bonds.[29] It should be mentioned that after successive coating of Fe_3O_4@SiO_2 with P4VP, the bands at 960 and 3740 cm^{-1} for free Si—OH groups are evacuated. Also the band at 468 cm^{-1} which is attributed to the Si—OH bending vibration is weakened after polymer coating.

Figure 3 shows the FE-SEM images and PSA photographs of Fe_3O_4, Fe_3O_4@SiO_2 and Fe_3O_4@SiO_2@P4VP nanoparticles. Fe_3O_4 nanoparticles were spherical and relatively mono-dispersed with an average diameter of 17 nm [Figure 3(a,d)]. After being coated with SiO_2 layer, the obtained nanoparticles had an average diameter of 40 nm [Figure 3(b,e)]. After successive coating with P4VP, a thin P4VP layer with an average thickness of 46 nm is deposited on the surface of the Fe_3O_4@SiO_2 nanospheres. So, final nanoparticles had average diameter of 86 nm [Figure 3(c,f)].

Figure 4 shows the transmission electron microscopy (TEM) image of Fe_3O_4@SiO_2@MPS@P4VP nanospheres. The core-shell structure of nanospheres with dark core and bright layer of shell is observed. Also, the particles have spherical shape and an average size of 90 nm.

Figure 5 displays the XRD pattern of Fe_3O_4 and Fe_3O_4@SiO_2@MPS@P4VP nanospheres. In Figure 5(a), characteristic diffraction peaks ($2\theta = 30.3°$, 35.8°, 43.5°, 53.9°, 57.6°, and 63°) indicates spinel structure indexes of Fe_3O_4 nanoparticles, respectively.[30] Also, it shows that the crystalline structure of Fe_3O_4 nanoparticles is face-centered cubic structure. After being coated with SiO_2 and P4VP, as shown in Figure 5(b), the main reflection of XRD patterns are the same as Fe_3O_4 reflections. Consistence of these curves (a and b in Figure 5) indicated that there is no crystal transition of the magnetic nanoparticles during silica coating and polymer grafting. As could be seen in Figure 5(b), an additional broad peak with the equivalent Bragg angle at $2\theta = 23°$ was recorded for Fe_3O_4@SiO_2@MPS@P4VP which demonstrates the presence of amorphous SiO_2 layer.[31]

The magnetization curves of Fe_3O_4 (a), Fe_3O_4@SiO_2 (b), and Fe_3O_4@SiO_2@MPS@P4VP (c) are shown in Figure 6. Hysteresis loops without remanence magnetization was investigated for all samples, indicating a superparamagnetic property.[32] The magnetic saturation of Fe_3O_4, Fe_3O_4@SiO_2, and Fe_3O_4@SiO_2@MPS@P4VP nanospheres is 49, 36, and 24 emu/g, respectively. Decrease of magnetic saturation value is due to coating of magnetic core with SiO_2 and P4VP layers. As a result, it would possible to easily separate the nanoparticles from solutions by applying magnetic field with a magnet.

Figure 7 shows TGA curves of MPS-modified Fe_3O_4@SiO_2 (a) and Fe_3O_4@SiO_2@MPS@P4VP (b) nanoparticles. In Figure 7, weight loss at temperatures less than 250 °C is related to evaporation of water and other solvents on the surface. The second stage of weight loss for Fe_3O_4@SiO_2@MPS, curve a, (about 5%) up to 450 °C is due to degradation of MPS organic groups. Also in Figure 7, the second stage of weight loss for Fe_3O_4@SiO_2@MPS@P4VP, curve b, (about 19%) is more than that of MPS-modified Fe_3O_4@SiO_2 nanoparticles, which demonstrate that successful grafting of P4VP onto the surface of MPS-modified Fe_3O_4@SiO_2 nanoparticles increased the content of organic groups.[33,34] According to Figure 7, it is suggested that the content of MPS groups and P4VP layer is about 5% and 14%, respectively. Also, the synthesized nanoparticles have thermal stability at below 250 °C.

The prepared magnetic nanoparticles after covalent attachment of P4VP can carry the positive charges after acidification. Thus, to evaluate the quantity of positive charges, zeta-potential measurement was conducted on the particles. Figure 8 shows the results of zeta potential measurements of the prepared particles before and after acidification procedure. Results confirm the

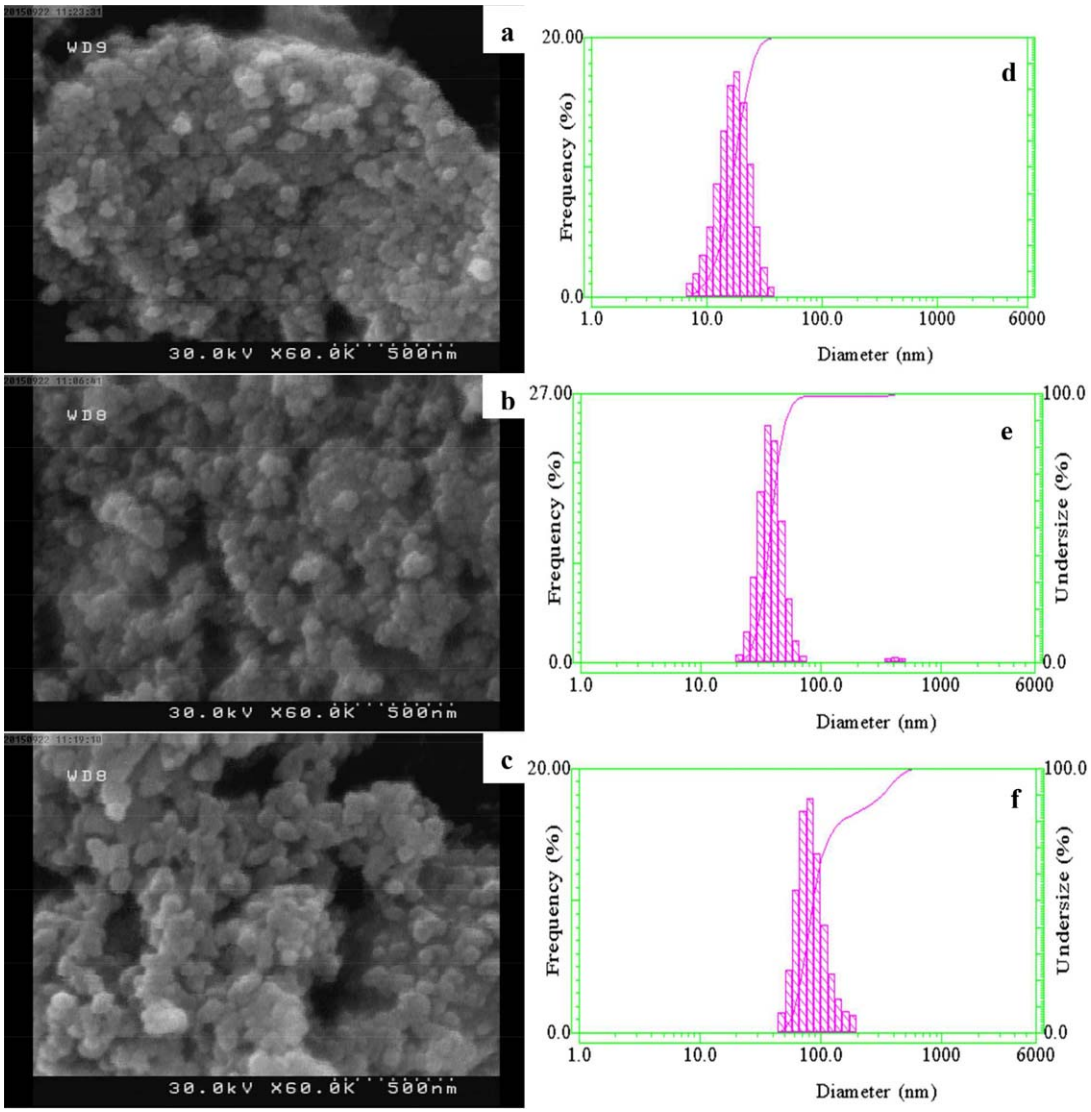

Figure 3. FE-SEM (a,b,c) and PSA photographs (d,e,f) of Fe_3O_4 (a,d), Fe_3O_4@SiO_2 (b,e), Fe_3O_4@SiO_2@P4VP (c,f). [Color figure can be viewed at wileyonlinelibrary.com.]

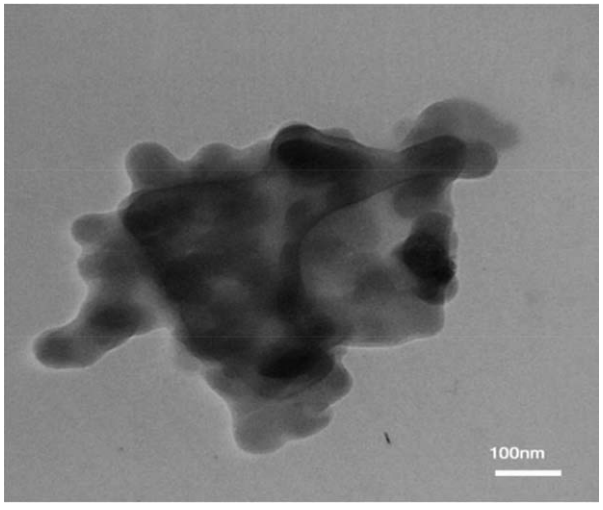

Figure 4. TEM image of Fe_3O_4@SiO_2@P4VP nanospheres.

presence of positive charges on the surface of Fe_3O_4@SiO_2@P4VP. As can be seen from this figure, before the introduction of positive charges onto the particles they were almost neutral (slightly positive with zeta potential of 6.2 mV). These slight positive charges can be attributed to the basic character of P4VP grafted to the magnetic particles.[35] But by contacting Fe_3O_4@SiO_2@P4VP particles with HCl (Figure 1), the particles' charges increased significantly (zeta potential of 78 mV).

Nitrate Removal Experiments

Effect of pH. pH is one of the most important parameters in the process of nitrate adsorption of protonated Fe_3O_4@SiO_2@P4VP. Experiments in specific conditions and pH range of 2–10 were performed to find the optimum pH. According to Figure 9, the best nitrate removal was achieved at pH 6. As seen in this figure, a slight fall of the nitrate removal was observed for Fe_3O_4@SiO_2@P4VP when pH decreases from 6.0 to 2.0.

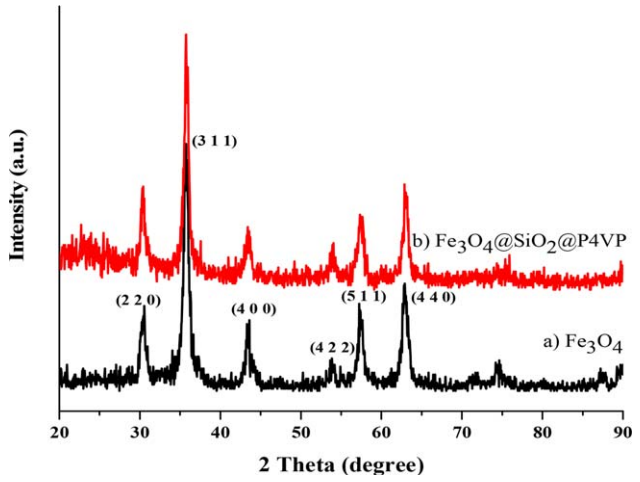

Figure 5. XRD pattern of (a) Fe_3O_4, (b) Fe_3O_4@SiO_2@MPS@P4VP. [Color figure can be viewed at wileyonlinelibrary.com.]

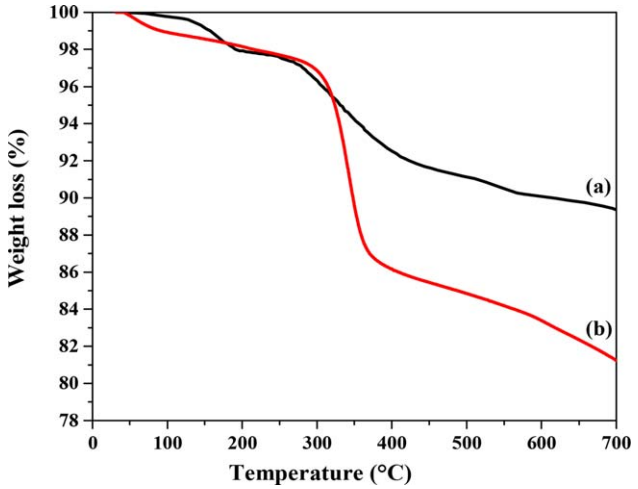

Figure 7. TGA curves of MPS-modified Fe_3O_4@SiO_2@MPS (a) and Fe_3O_4@SiO_2@P4VP (b). [Color figure can be viewed at wileyonlinelibrary.com.]

Because, large amounts of Cl^- might compete with nitrate ions exchange. In contrast, at higher values of pH, (pH > 6) the removal efficiency decreased abruptly. This is probably associated with the decreased protonation of P4VP ($pK_a = 5.2$).[36] By increasing the pH, anion exchanging groups of the polymer (positively charged pyridyl groups) are deprotonated; hence, P4VP chains grafted to the magnet cores tend to bend and entangle with each other at pH ≫ pKa to form a compact conformation with reduction of the hydrodynamic size from about 300 to 100 nm for completely charged to uncharged particles (Results not shown). Therefore, the hydrophobic nature of P4VP due to the uncharged pyridyl groups as well as alkyl groups in the main chains attached to the magnetic particles made them hydrophobic with WCA of 130° in the neutralization form (Figure 10).

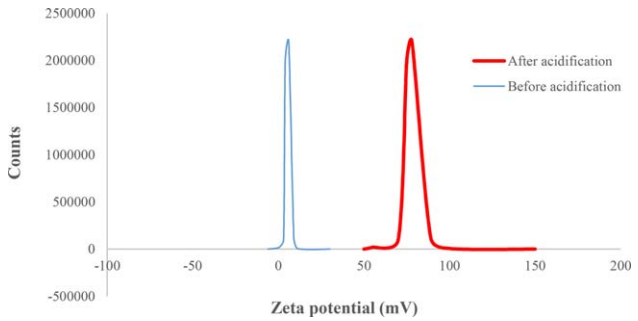

Figure 8. Zeta potential distribution curves for the Fe_3O_4@SiO_2@P4VP solution before and after acidification. [Color figure can be viewed at wileyonlinelibrary.com.]

Effect of Contact Time. To investigate the effect of contact time on nitrate removal, experiments in the interval of 10–180 min were performed. The results are shown in Figure 11. In the beginning, many active sites are prepared to adsorb nitrate ions. With increasing time, these sites are saturated and reduced nitrate adsorption. According to Figure 11, the maximum of

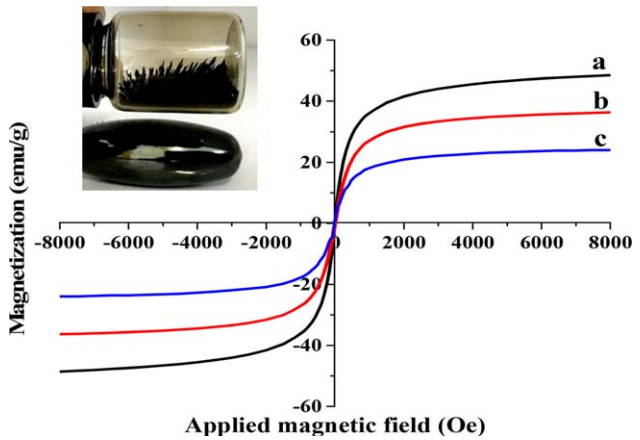

Figure 6. Magnetization curves of Fe_3O_4 (a), Fe_3O_4@SiO_2 (b), and Fe_3O_4@SiO_2@MPS@P4VP (c). [Color figure can be viewed at wileyonlinelibrary.com.]

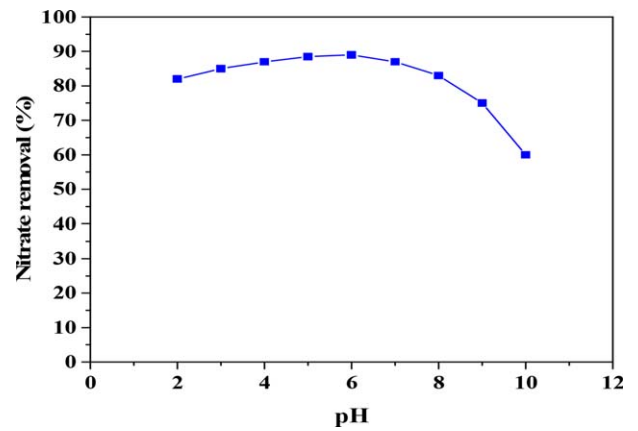

Figure 9. Effect of pH on nitrate removal (initial nitrate concentration, 100 mg/L). [Color figure can be viewed at wileyonlinelibrary.com.]

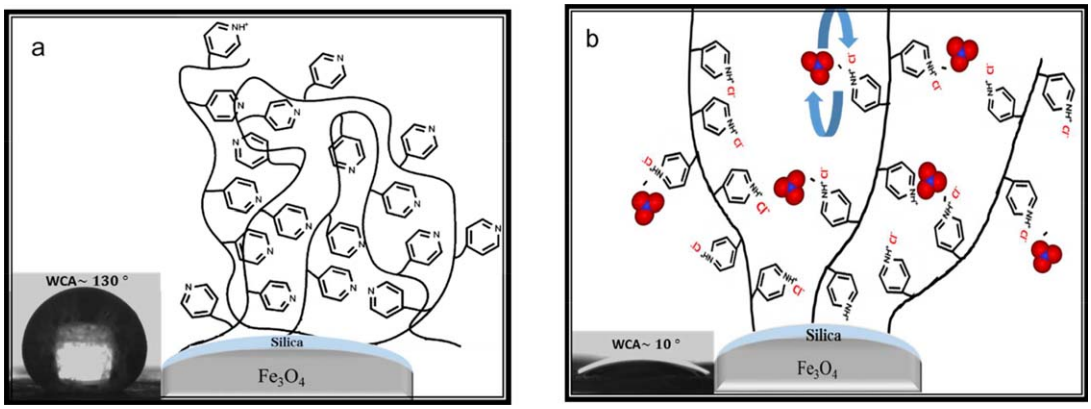

Figure 10. The change in conformation of the polymeric layer and wettability alteration in Fe_3O_4@SiO_2@P4VP particles before (a) and after (b) acidification. [Color figure can be viewed at wileyonlinelibrary.com.]

nitrate removal was obtained within 100 min, and then no significant changes were observed for the following 80 min. The obtained result shows better performance of the prepared nanoparticles compared to similar systems. Saad *et al.*[37] synthesized three different ammonium-functionalized mesoporous silica for nitrate removal and they reported 3 h as equilibrium time of adsorption. Bekhradinassab *et al.*[38] immobilized nanoscale zerovalent iron (NZVI) on SiO_2-FeOOH cores for removing nitrate from drinking water and equilibrium time was about 2.5 h.

Effect of Sorbent Dosage. Figure 12 shows the effect of sorbent added to the nitrate solution. Various amount (10–80 mg) of synthesized sorbent were added to nitrate solutions and mass of adsorbed nitrate for each solution was determined. It was seen that increasing the amount of sorbent dosage up to 50 mg, increased the nitrate adsorption and after adding a 50 mg sorbent, nitrate uptake reached equilibrium.

Adsorption Isotherms Modeling

To investigate the equilibrium adsorption of synthesized sorbent, experiments were done in different initial concentrations of nitrate solutions (50–500 mg/L) under optimal conditions (i.e., pH: 6, contact time: 100 min, and sorbent dosage: 50 mg) and the volume of the nitrate solutions was 10 mL. Then, the results were evaluated by Langmuir and Freundlich isotherm models. Figure 13 shows the fitted experimental data with both models. The constants and correlation coefficient (R^2) of both models are summarized in Table I. As seen, the Langmuir model could better describe the adsorption of nitrate by synthesized sorbent. This implies monolayer coverage of nitrate ion on the surface of sorbent.[39] This would be reasonable that the $-NH^+$ groups are the major functional groups in the adsorption process and there is no interaction between sorbed nitrate ions. Also, the maximum adsorption capacity of 80.6 (mg nitrate/g sorbent) is expected, Comparison of the obtained capacities to the amount of grafted 4-vinylpyridine groups on the Fe_3O_4@-SiO_2 surface (1.45 mmol/g) depicts that, at most, only 84% of the grafted groups were involved in the nitrate adsorption. This may be attributed to the incomplete protonation of the 4VP groups grafted on the magnetic cores.

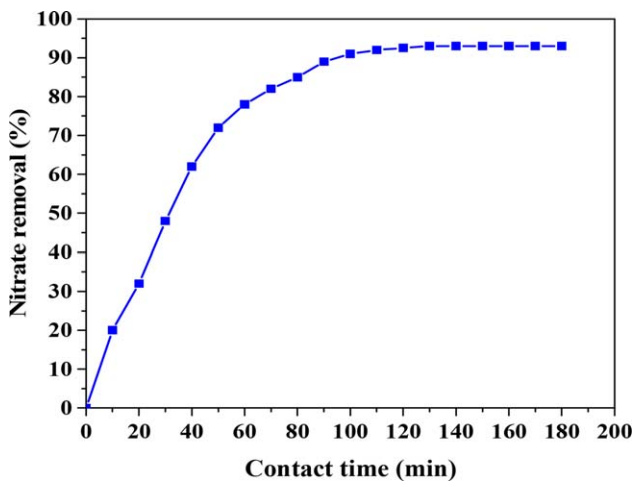

Figure 11. Effect of contact time on nitrate removal ($C_0 = 100$ mg/L, pH = 6). [Color figure can be viewed at wileyonlinelibrary.com.]

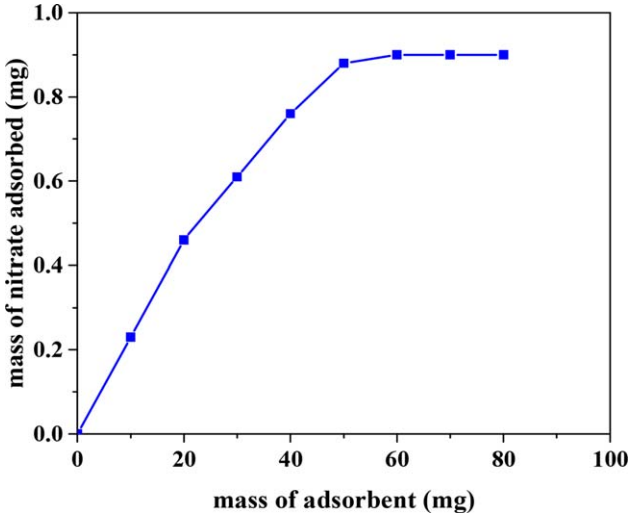

Figure 12. Effect of sorbent dosage on nitrate adsorption mass (C_0:100 mg/L, pH = 6, and contact time = 100 min). [Color figure can be viewed at wileyonlinelibrary.com.]

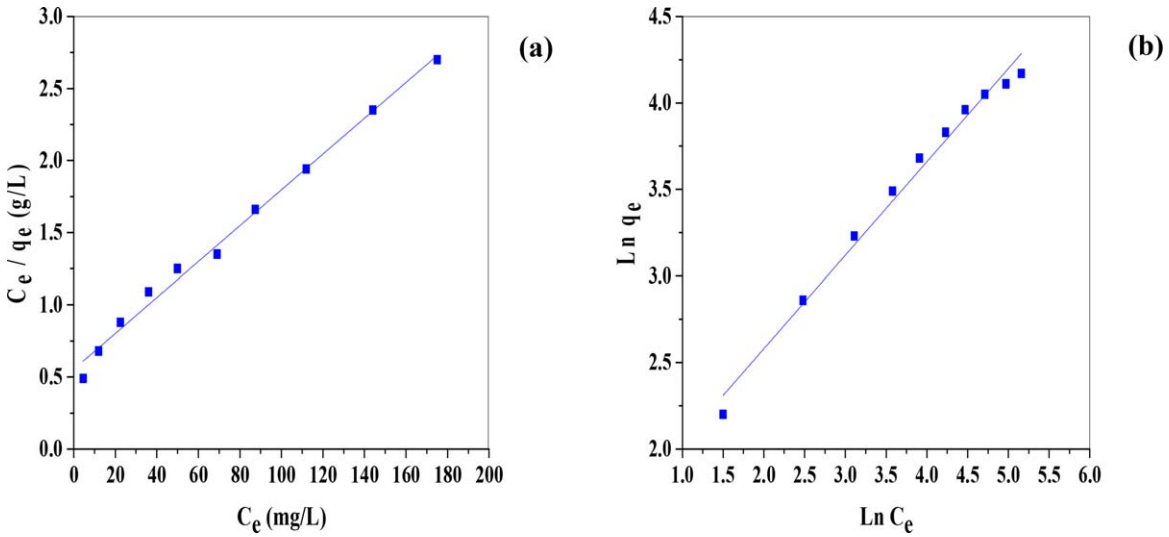

Figure 13. Langmuir (a) and Freundlich (b) isotherms of nitrate adsorption. Experimental conditions: initial concentration of nitrate solutions 50–500 mg/L, pH: 6, contact time: 100 min, and sorbent dosage: 50 mg. [Color figure can be viewed at wileyonlinelibrary.com.]

Table I. Adsorption Isotherms Parameters

Langmuir isotherm			Freundlich isotherm		
q_{max}	a_L	R^2	n	K_F	R^2
80.6	0.0224	0.9924	1.85	4.48	0.9872

The essential features of the Langmuir isotherm can be expressed in terms of the dimensionless equilibrium parameter, R_L, which is defined as:

$$R_L = \frac{1}{1 + a_L C_i} \quad (8)$$

where a_L is the Langmuir constant as described above and C_i is initial concentration (mg/L). The value of R_L indicated the shape of Langmuir isotherm to be irreversible ($R_L = 0$), linear ($R_L = 1$), unfavorable ($R_L > 1$), or favorable ($0 < R_L < 1$).[40] In the present work, initial concentration of nitrate is 100 mg/L and value of a_L according to Table I is 0.0224 (L/g). So, the R_L value in the present work was found to be 0.308, indicating favorable adsorption of the nitrate ions onto sorbent.

The relatively low value of correlation coefficient ($R^2 = 0.9872$) for Freundlich isotherm shows that the adsorption process occurs mainly by the ionic interactions between nitrate anions and NH^+ cations on the surface of sorbent, so adsorption process is not much heterogeneous.[41] According to Mckay *et al.*[40] the value of n (Freundlich constant) in the range of $1 < n < 10$ can represent a good adsorption. In the present study, as n lies between 1 and 10 ($n = 1.85$) it indicates beneficial adsorption of nitrate onto Fe_3O_4@SiO_2@P4VP nanosorbent.

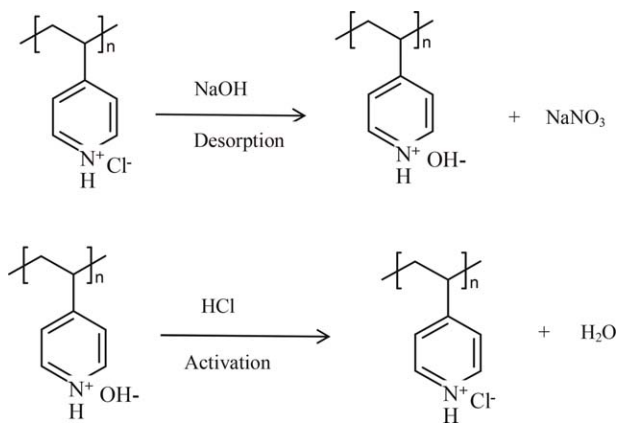

Figure 14. Desorption and activation of the pyridyl groups to regenerate Fe_3O_4@SiO_2@P4VP nanosorbent.

Desorption and Regeneration

To check the desorption of nitrate ions from sorbent surface, the saturated sorbent washed with 0.01 *M* NaOH solution for 10 min. Afterward the adsorbent was entered to HCl solution (0.1 mol/L) to activate positive charges on surface (Figure 14). Then, the regenerated sorbent dried and was placed in contact with nitrate solution. After four adsorption–desorption cycles, as one can see in Figure 15, the efficiency of sorbent was not significantly reduced (about 9%). Therefore, the synthesized sorbent could use as efficient and cost effective sorbent.

CONCLUSIONS

In the present work, Fe_3O_4@SiO_2@MPS@P4VP nanospheres were synthesized and proved to be an efficient sorbent for removal of nitrate ions from aqueous solutions. Different analyzes including FTIR spectra, FE-SEM and TEM images, XRD pattern, VSM, and TGA indicated successful synthesis of nanospheres. Effective parameters on nitrate adsorption pH, contact time, and sorbent dosage were optimized. The adsorption data were evaluated by Langmuir and Freundlich isotherm models. The results showed that Langmuir model could better describe

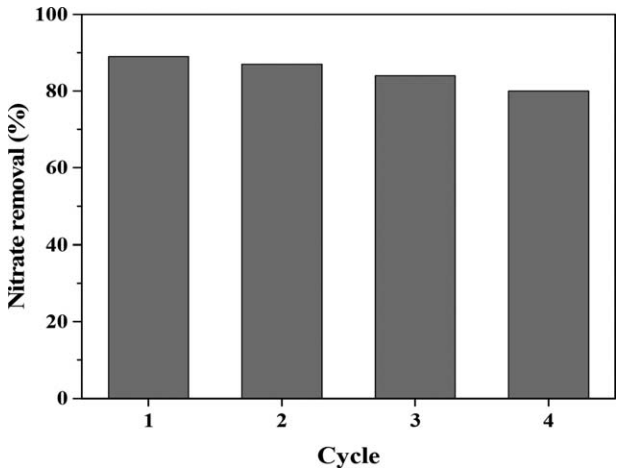

Figure 15. Desorption performance of synthesized sorbent.

the adsorption of nitrate ions and the maximum expectance adsorption capacity was 80.6 (mg nitrate/g sorbent). The desorption of the synthesized sorbent achieved within 10 min using 0.01 *M* NaOH solution. Also, the efficiency of sorbent was not significantly reduced (about 9%) after four adsorption–desorption cycles.

ACKNOWLEDGMENTS

Authors would like to acknowledge School of Chemical and Petroleum Engineering, Nanotechnology Research Institute and Department of Chemistry at Shiraz University.

REFERENCES

1. Loganathan, P.; Vigneswaran, S.; Kandasamy, J. *J. Environ. Manag.* **2013**, *131*, 363.
2. Zhan, Y.; Lin, J.; Zhu, Z. *J. Hazard. Mater.* **2011**, *186*, 1972.
3. Bhatnagar, A.; Sillanpää, M. *Chem. Eng. J.* **2011**, *168*, 493.
4. World Health Organization, Guidelines for Drinking-Water Quality, 4th ed.; World Health Organization: Geneva, Switzerland, **2011**.
5. Li, Y.; Lin, X.; Zhuo, X.; Luo, X. *J. Appl. Polym. Sci.* **2013**, *128*, 2746.
6. Ahn, J. H.; Choo, K. H.; Park, H. S. *J. Membr. Sci.* **2008**, *310*, 296.
7. Oh, C. M.; Hwang, C. W.; Hwang, T. S. *J. Environ. Chem. Eng.* **2014**, *2*, 2162.
8. Epsztein, R.; Nir, O.; Lahav, O.; Green, M. *Chem. Eng. J.* **2015**, *279*, 372.
9. Govindan, K.; Noel, M.; Mohan, R. *J. Water Process Eng.* **2015**, *6*, 58.
10. Kumar, M.; Chakraborty, S. *J. Hazard. Mater.* **2006**, *135*, 112.
11. Soares, M. I. M. *Water Air Soil Pollut.* **2000**, *123*, 183.
12. Worch, E. Adsorption Technology in Water Treatment: Fundamentals, Processes, and Modeling; Walter de Gruyter, GmbH & Co. KG: Berlin/Germany, **2012**.
13. Poursaberi, T.; Karimi, M.; Hassanisadi, M.; Sereshti, H. *J. Porphyr. Phthalocyanines* **2013**, *17*, 359.
14. Ghasemi, E.; Sillanpää, M. *J. Sep. Sci.* **2015**, *38*, 164.
15. Nabid, M. R.; Sedghi, R.; Sharifi, R.; Oskooie, H. A.; Heravi, M. M. *Iran. Polym. J.* **2013**, *22*, 85.
16. Neagu, V.; Mikhalovsky, S. *J. Hazard. Mater.* **2010**, *183*, 533.
17. Tamami, B.; Farjadian, F. *J. Iran. Chem. Soc.* **2011**, *8*, S77.
18. Shi, P.; Gao, C.; He, X.; Sun, P.; Zhang, W. *Macromolecules* **2015**, *48*, 1380.
19. Meng, F.; Zhang, W.; Zheng, S. *J. Mater. Sci.* **2005**, *40*, 6367.
20. Huang, A.; Xiao, C.; Zhuang, L. *J. Appl. Polym. Sci.* **2005**, *96*, 2146.
21. Tamami, B.; Goudarzian, N. *Eur. Polym. J.* **1992**, *28*, 1035.
22. Khaligh, N. G.; Ghasem-Abadi, P. G.; Mihankhah, T. *C. R. Chim.* **2014**, *17*, 23.
23. Loekitowati Hariani, P.; Faizal, M.; Ridwan, R.; Marsi, M.; Setiabudidaya, D. *Int. J. Environ. Sci. Dev.* **2013**, *4*, 336.
24. Stöber, W.; Fink, A.; Bohn, E. *J. Colloid Interface Sci.* **1968**, *26*, 62.
25. Yuan, Q.; Li, N.; Chi, Y.; Geng, W.; Yan, W.; Zhao, Y.; Li, X.; Dong, B. *J. Hazard. Mater.* **2013**, *254*, 157.
26. Cao, N.; Zhao, Y.; Sang, B.; Wang, Z.; Cao, L.; Sun, L.; Zou, X. *Mater. Sci. Eng. C* **2016**, *69*, 330.
27. Chen, D.; Hu, B.; Huang, C. *Talanta* **2009**, *78*, 491.
28. Pei, Y.; Han, Q.; Tang, L.; Zhao, L.; Wu, L. *Mater. Technol.* **2016**, *31*, 38.
29. Guo, W.; Wang, Q.; Luan, Y.; Wang, G.; Dong, W.; Yu, J. *Chem. Asian J.* **2015**, *10*, 701.
30. Chen, Z.; Yang, Q.; Peng, K.; Guo, Y. *J. Appl. Polym. Sci.* **2011**, *119*, 3582.
31. An, N.; Lin, H.; Yang, C.; Zhang, T.; Tong, R.; Chen, Y.; Qu, F. *Mater. Sci. Eng. C* **2016**, *69*, 292.
32. Rutnakornpituk, B.; Wichai, U.; Vilaivan, T.; Rutnakornpituk, M. *J. Nanopart. Res.* **2011**, *13*, 6847.
33. Cheng, H. L.; Miao, L.; Su, L. F.; Tanemura, S.; Xu, G. *Key Eng. Mater.* **2012**, *512*, 563.
34. Lu, L.; Wang, W.; Cai, W.; Chen, Z. R. *J. Appl. Polym. Sci.* **2013**, *128*, 4130.
35. Roach, J. D.; Lane, R. F.; Hussain, Y. *Water Res.* **2011**, *45*, 1387.
36. Escalé, P.; Rubatat, L.; Derail, C.; Save, M.; Billon, L. *Macromol. Rapid Commun.* **2011**, *32*, 1072.
37. Saad, R.; Hamoudi, S.; Belkacemi, K. *J. Porous Mater.* **2008**, *15*, 315.
38. Ensie, B.; Samad, S. *Desalination* **2014**, *347*, 1.
39. Hamoudi, S.; Saad, R.; Belkacemi, K. *Ind. Eng. Chem. Res.* **2007**, *46*, 8806.
40. Mckay, G.; Blair, H.; Gardner, J. *J. Appl. Polym. Sci.* **1982**, *27*, 3043.
41. Chatterjee, S.; Woo, S. H. *J. Hazard. Mater.* **2009**, *164*, 1012.